JACS
JOURNAL OF THE AMERICAN CHEMICAL SOCIETY
Article
pubs.acs.org/JACS

In Vivo and *in Situ* Tracking Cancer Chemotherapy by Highly Photostable NIR Fluorescent Theranostic Prodrug

Xumeng Wu,[†] Xuanrong Sun,[‡] Zhiqian Guo,*[,†] Jianbin Tang,*[,‡] Youqing Shen,[‡] Tony D. James,[⊥] He Tian,[†] and Weihong Zhu*[,†]

[†]Key Laboratory for Advanced Materials and Institute of Fine Chemicals, Shanghai Key Laboratory of Functional Materials Chemistry, East China University of Science and Technology, Shanghai 200237, China

[‡]Key Laboratory of Biomass Chemical Engineering of Ministry of Education, Center for Bionanoengineering, and Department of Chemical and Biological Engineering, Zhejiang University, Hangzhou, Zhejiang, 310027, China

[⊥]Department of Chemistry, University of Bath, Bath BA2 7AY, United Kingdom

Supporting Information

ABSTRACT: *In vivo* monitoring of the biodistribution and activation of prodrugs is urgently required. Near infrared (NIR) fluorescence-active fluorophores with excellent photostability are preferable for tracking drug release *in vivo*. Herein, we describe a NIR prodrug DCM-S-CPT and its polyethylene glycol−polylactic acid (PEG-PLA) loaded nanoparticles as a potent cancer therapy. We have conjugated a dicyanomethylene-4*H*-pyran derivative as the NIR fluorophore with camptothecin (CPT) as the anticancer drug using a disulfide linker. *In vitro* experiments verify that the high intracellular glutathione (GSH) concentrations in tumor cells cause cleavage of the disulfide linker, resulting in concomitantly the active drug CPT release and significant NIR fluorescence turn-on with large Stokes shift (200 nm). The NIR fluorescence of DCM-S-CPT at 665 nm with fast response to GSH can act as a direct off−on signal reporter for the GSH-activatable prodrug. Particularly, DCM-S-CPT possesses much better photostability than ICG, which is highly desirable for *in situ* fluorescence-tracking of cancer chemotherapy. DCM-S-CPT has been successfully utilized for *in vivo* and *in situ* tracking of drug release and cancer therapeutic efficacy in living animals by NIR fluorescence. DCM-S-CPT exhibits excellent tumor-activatable performance when intravenously injected into tumor-bearing nude mice, as well as specific cancer therapy with few side effects. DCM-S-CPT loaded in PEG-PLA nanoparticles shows even higher antitumor activity than free CPT, and is also retained longer in the plasma. The tumor-targeting ability and the specific drug release in tumors make DCM-S-CPT as a promising prodrug, providing significant advances toward deeper understanding and exploration of theranostic drug-delivery systems.

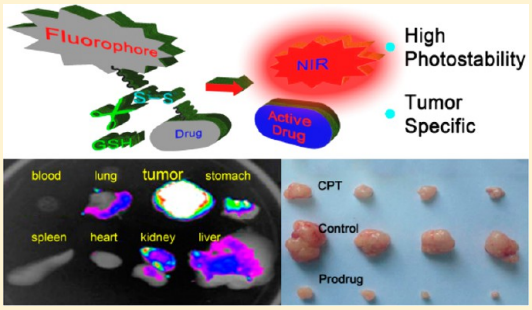

INTRODUCTION

Chemotherapy as a dominant treatment modality against cancer is hindered by its severe side-effects to normal cells and tissues because of its nonselectivity and high toxicity.[1−8] Developing controllable drug delivery systems (DDS),[9−12] which can be triggered by the unique tumor microenvironment, is one of the most promising strategies to enhance the selectivity and thus significantly improve the therapeutic efficacy of anticancer drugs.[13−19] Given that cancer cells have much higher intracellular glutathione (GSH) concentration than normal cells and tissues,[20−23] a variety of GSH-activatable prodrugs with disulfide bond linkage have been constructed with promising therapeutic efficacy.[24−27] However, *in situ* tracking of the biodistribution and release for the activated drug specifically in tumors is still urgently required, but remains challenging.[28−31] Indeed, developing a method for the *in situ* tracking of prodrugs after *in vivo* uptake, particularly in a noninvasive manner, is of critical importance.

Theranostic prodrugs equipped with fluorophores as optical reporters have become attractive to monitor the drug delivery and release process since their fluorescence signals can be activated concomitantly with drug release.[26,32−34] It would be desirable to utilize near-infrared (NIR) fluorophores as the signaling subunit in prodrugs because NIR photons can deeply penetrate the skin and underlying tissue with minimal damage to the biological samples with low background interference.[35−49] To date, most of the fluorophores used for theranostic prodrugs, such as coumarin,[50] 1,8-naphthalimide,[51,52] and xanthene,[32] suffer from short wavelength emission. Therefore, the *in vivo* drug release performance could only be predicted indirectly *via in vitro* experiments. Even with the utilization of cyanine dye[53] as the optical NIR reporter in a prodrug, there is still a lack of tracking of the drug release *in vivo* and *in situ*, which is most probably ascribed to the poor

Received: December 5, 2013
Published: February 13, 2014

   dx.doi.org/10.1021/ja412380j | J. Am. Chem. Soc. 2014, 136, 3579−3588

photostability of cyanines.[54−56] Undoubtedly, photostability of the NIR fluorophores is another key design element for constructing theranostic prodrugs for the real-time monitoring of drug delivery and therapeutic efficacy *in vivo*.

Novel NIR-active fluorophores with excellent photostability and photophysical properties are preferable for tracking drug release *in vivo*. As donor−π−acceptor (D−π−A) structured chromophore, dicyanomethylene-4*H*-pyran (DCM) derivatives have attracted considerable attention owing to their attractive features such as controllable emission wavelength in the NIR region *via* tuning electron donor ability, large Stokes shift from the ultrafast intramolecular charge transfer (ICT), and high photostability.[57−59] Actually, a myriad of approaches have been devoted to develop DCM-based nonlinear optic materials,[60] fluorescent sensors,[61,62] logic gates,[63−65] and photovoltaic sensitizers.[66,67] Surprisingly, DCM derivatives are rarely employed in drug delivery systems. Herein we describe a novel NIR DCM-based theranostic prodrug platform for cancer treatment *in vivo* with high photostability. The prodrug, DCM-S-CPT (Scheme 1), is composed of camptothecin (CPT), an inhibitor of topoisomerase I as the activatable anticancer drug,[68,69] and the DCM moiety as the NIR fluorescence reporter. The two units are linked by a disulfide linker ("S−S") that could be cleaved by biologically abundant reducing thiols such as GSH.[70−76] We focused our investigations on the *in situ* tracking as well as *in vivo* antitumor activities of DCM-S-CPT and corresponding polyethylene glycol−polylactic acid (PEG-PLA) nanoparticles.[77−79] This developed NIR theranostic prodrug platform bestows several striking characteristics: (i) significant turn-on of NIR fluorescence along with GSH-induced release of active CPT; (ii) significantly better photostability than commercially available cyanine dye ICG (19-fold enhancement in the half-life of fluorescence) which is convenient for *in situ* tracking; (iii) extremely high inhibition rates of tumor growth (IRT) with lower side-effects. To the best of our knowledge, DCM-S-CPT is the first NIR DCM-based prodrug which can be implemented for *in situ* and *in vivo* tracking of antitumor chemotherapy in living animal models. DCM-S-CPT can be applied as a prodrug upon GSH-induced disulfide bond cleavage in a drug-delivery system, along with high selectivity over other biological interferences, including metal ions. Its long NIR wavelength and high photostability make significant advances toward deeper understanding and exploring theranostic drug-delivery systems. Most importantly, the tumor-targeting ability and the specific drug release in tumors make DCM-S-CPT a promising prodrug with high efficacy and reduced side-effects.

Scheme 1. Chemical Structures of Activatable Prodrug DCM-S-CPT, Nonactivatable Control DCM-C-CPT and Commercially Available ICG

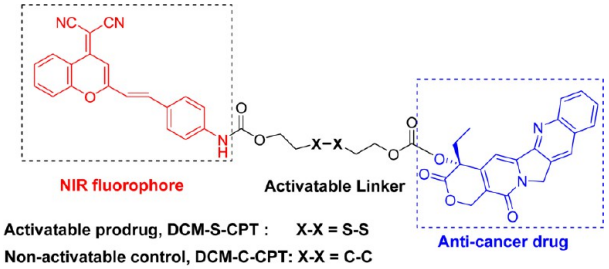

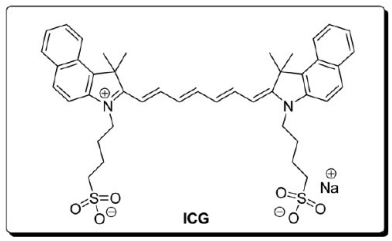

RESULTS AND DISCUSSION

Design and Synthesis. The synthetic route for prodrug DCM-S-CPT is depicted in Scheme S1 in the Supporting Information (SI). The key intermediate compound 2-(2-methyl-4*H*-chromen-4-ylidene) malononitrile (DCM) was synthesized according to the establsihed procedures.[80,81] DCM-NH_2 was prepared by the reaction of DCM with PhN_3[82] in toluene, during which the azide unit is spontaneously reduced to amino group. Then, DCM-NH_2 was reacted with triphosgene in the presence of *N*,*N*′-diisopropylethylamine (DIEA), and followed by treatment with 2,2′-dithiodiethanol to generate DCM-S in toluene. Finally, the target prodrug DCM-S-CPT was obtained from the reaction of chloroformate of CPT and DCM-S at room temperature.[83] Meanwhile, as a control system, an uncleavable linker ("C−C") was employed in DCM-C-CPT (Scheme 1). The prodrugs were further loaded into a biodegradable PEG-PLA micelle in order to improve their solubility in water and achieve enhanced permeability and retention (EPR).[84−87] The PEG-PLA micelles loaded with either DCM-S-CPT or DCM-C-CPT (PEG-PLA/DCM-S-CPT or PEG-PLA/DCM-C-CPT) had an average size of 44 nm with PDI (polydispersion index) of 0.429, and 79 nm with PDI of 0.288, respectively (Figure S1 in SI).

GSH-Activatable Properties. Owing to its D−π−A structure, DCM-S-CPT exhibits a typical ICT broad absorption band at 455 nm with fairly weak emission at 665 nm in DMSO/PBS buffer solution (50/50, v/v, pH = 7.4, 10 mM) (Figure 1). On the other hand, DCM-NH_2 has a strong NIR fluorescence at 665 nm in the same condition with the absorption band at 492 nm (Figure S2A in SI). The distinct difference between DCM-NH_2 and DCM-S-CPT in the spectroscopic properties can be attributed to the masking of the electron-withdrawing amide bond in DCM-S-CPT, along with disruption of the electron donating ability of the nitrogen atom. Notably, there is no sign of the blue fluorescence from CPT in this prodrug upon excitation at 365 nm (Figure S4 in SI).[88] Considering the substantial overlaps of donor (CPT) emission and acceptor (DCM moiety) absorption bands in DCM-S-CPT, the quenched fluorescence of CPT moiety could be ascribed to the intramolecular fluorescence resonance energy transfer (FRET, Figure S3 in SI).[89,90] This is also indicative of the successful conjugation of DCM and CPT moieties.

To test our system containing an activatable disulfide linker, the spectral properties of prodrug DCM-S-CPT upon reaction with GSH were investigated. As expected, the prodrug DCM-S-CPT produced both colorimetric and fluorescence spectral changes upon addition of GSH in DMSO/PBS solution (50/50, v/v, pH = 7.4, 10 mM). Upon the treatment with 2.5 mM GSH, the absorption band shifted to 492 nm with a 37 nm red-shift, accompanied by a color change from pale yellow to pink (Figure 1A). More importantly, this activated a significant NIR fluorescence at 665 nm, which was enhanced by about 10-fold upon excitation at the isosbestic point of 465 nm, and exhibited a linear increase with GSH concentration (0−200 μM, Figure

dx.doi.org/10.1021/ja412380j | J. Am. Chem. Soc. 2014, 136, 3579−3588

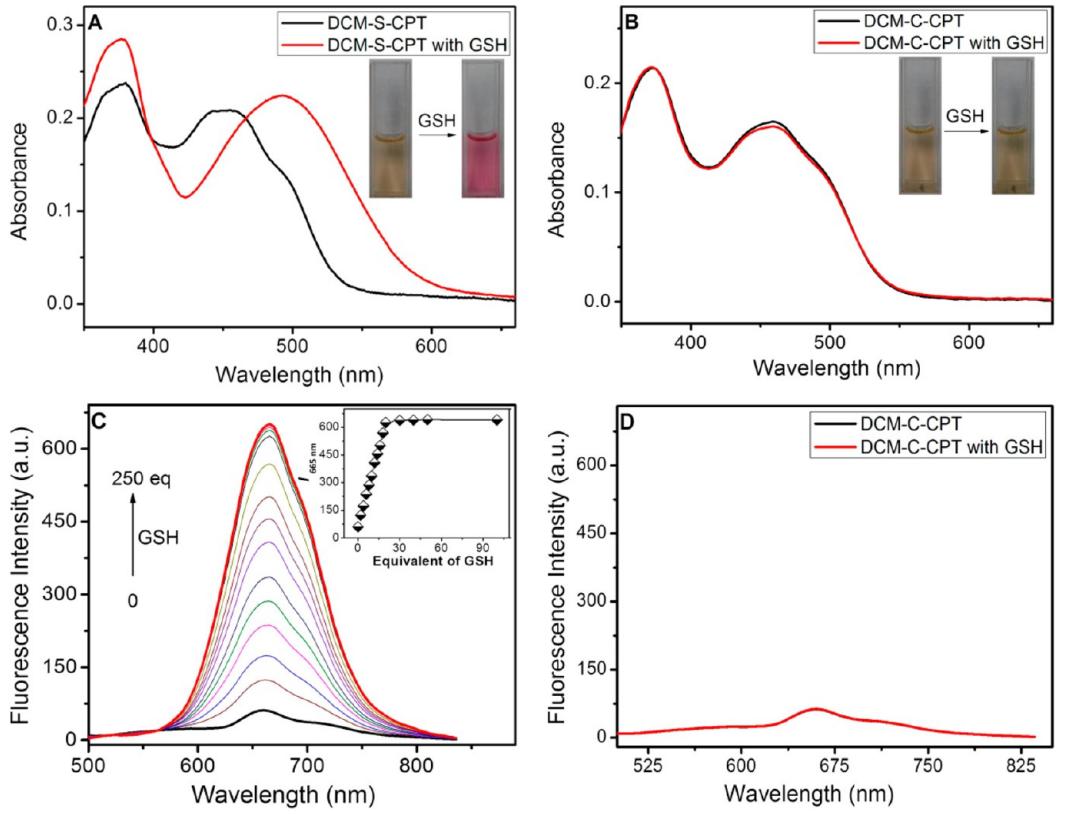

Figure 1. Absorption and emission changes of (A, C) activatable prodrug DCM-S-CPT (10 μM) and (B, D) control DCM-C-CPT (10 μM) in the presence of GSH (2.5 mM, 250 equiv) in DMSO/PBS solution (50/50, v/v, pH = 7.4, 10 mM). Inset (A) and (B): Color changes observed from solution of DCM-S-CPT and DCM-C-CPT upon addition of GSH. Inset (C): fluorescence intensity at 665 nm ($I_{665\ nm}$) of DCM-S-CPT as a function of GSH. Each point was recorded after exposure to GSH for 1 h at 37 °C, λ_{ex} = 465 nm. Note: Here the isosbestic point of 465 nm is chosen as the excitation wavelength for the sake of keeping the same light absorbance to exactly compare the turn-on fluorescence before and after the GSH-induced cleavage of the disulfide bond.

1C). Conversely, the control DCM-C-CPT with alkane bonds ("C−C") as linker displays almost no change of photophysical properties upon treatment with GSH (Figure 1B and D). The distinctly different spectroscopic response of DCM-S-CPT and DCM-C-CPT to GSH also indicates that the optical response of DCM-S-CPT as well as the release of CPT is derived from the cleavage of the disulfide linker by biological thiols such as GSH. Meanwhile, after the treatment of DCM-S-CPT with GSH, the fluorescence centered at 436 nm originating from the CPT moiety is also recovered (Figure S4 in SI), clearly indicating that cleavage of the disulfide bond in DCM-S-CPT interrupts the intramolecular FRET process.

Subsequently, the spectra of free DCM-NH_2 were compared with DCM-S-CPT after the treatment with GSH (Figure S2 in SI). The identical positions and shapes indicate that DCM-NH_2 is the product and NIR fluorescence emitter produced when GSH was added to the DCM-S-CPT system (Scheme 2). Moreover, the anticipated release of CPT as active cancer drug was also proven by ESI-MS analyses. Upon interaction of 20 equiv of GSH with DCM-S-CPT, peaks of 349.1 (corresponding to $[CPT + H]^+$) and 312.1 (corresponding to $[DCM\text{-}NH_2 + H]^+$) were observed simultaneously in the high resolution MS spectrum (HRMS, Figure S5 in SI), clearly indicating that the active CPT can be released from the prodrug DCM-S-CPT upon exposure to GSH, with concomitant generation of the NIR reporter DCM-NH_2 by a two-step reaction (cleavage of disulfide bond and then an intramolecular cyclization, Scheme 2).[91] Notably, for DCM-S-CPT, the fluorescence of DCM-NH_2 falls into the NIR region (650−900 nm), particularly preferable for *in vivo* bioimaging because of the deep penetration ability and low background autofluorescence. Furthermore, the

Scheme 2. Proposed CPT Release Mechanism of the Activatable Prodrug by Treatment of GSH

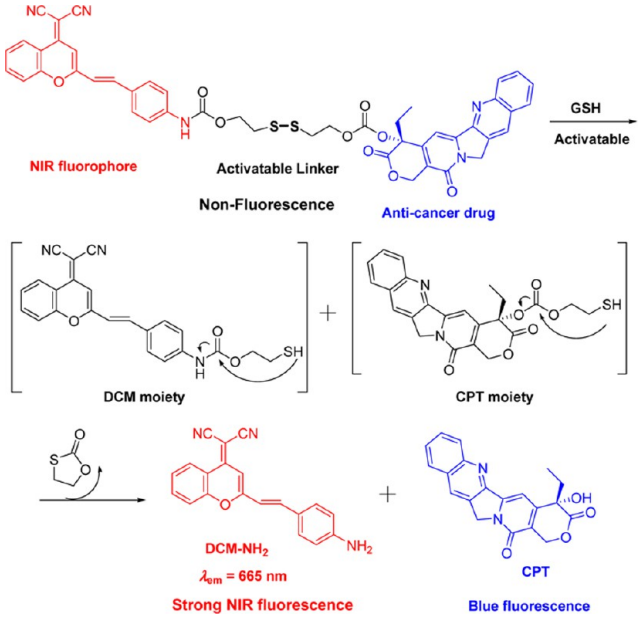

dx.doi.org/10.1021/ja412380j | J. Am. Chem. Soc. 2014, 136, 3579−3588

significant Stokes shift of 200 nm, resulting from the intramolecular charge transfer from amino (donor) to DCM unit (acceptor), is desirable for high quality optical imaging because it enhances the signal fidelity.[92−94]

To evaluate the possible application of DCM-S-CPT in real biological systems, the performance of DCM-S-CPT with other biologically relevant analytes such as amino acids and abundant metal ions was investigated (Figure 2A). Upon exposure to 1,4-dithiothreitol (DTT), cysteine (Cys), and homocysteine (Hcy), similar spectroscopic response of DCM-S-CPT as with GSH could be observed due to their thiol-containing structures. On the other hand, no appreciable fluorescence enhancement could be induced by treatment with other nonthiol amino acids and metal ions, confirming the specific cleavage of the disulfide bond elicited by thiol-containing species (Figure 2A). Actually, the potential interference of DTT, Cys, and Hcy can be neglected due to their relatively low concentration in contrast to that with high physiological concentration of GSH in cytoplasm (1−15 mM).[26,95] The pH effect on the GSH-induced fluorescence changes of DCM-S-CPT at 665 nm was also investigated. As shown in Figure 2B, DCM-S-CPT remains stable and nonfluorescent within a pH range of 3.5−9, and possesses aforementioned activatable fluorescence response to GSH upon changing the pH from 6 and 9. Accordingly, DCM-S-CPT can be applied as a prodrug upon GSH-induced disulfide bond cleavage in drug-delivery systems, together with high selectivity over various other potential biological interference, including metal ions.

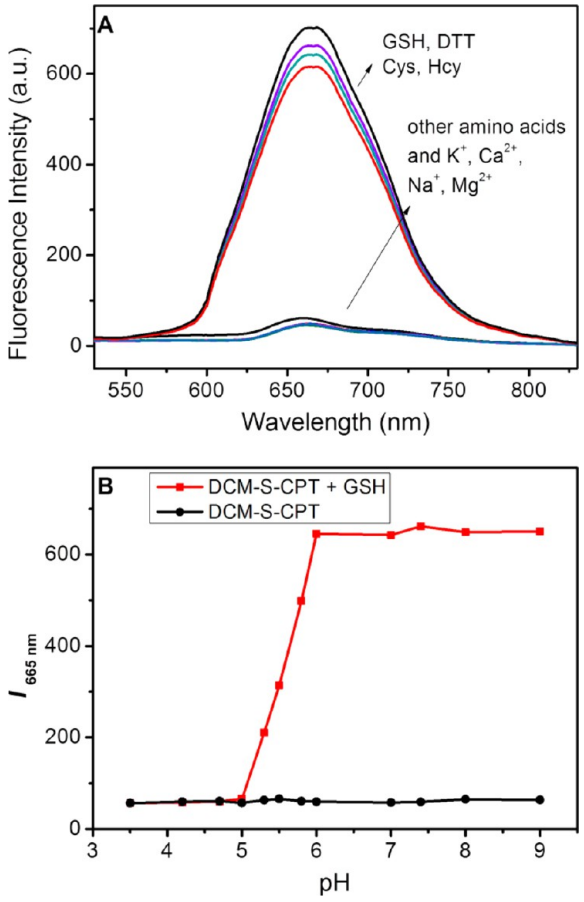

Figure 2. (A) Fluorescence response of DCM-S-CPT (10 μM) upon addition of 2.5 mM GSH, DTT, Cys, Hcy, K^+, Ca^{2+}, Na^+, Mg^{2+}, and other amino acids including Ala, Arg, Asn, Asp, Gln, Glu, Gly, His, Ile, Leu, Phe, Pro, Ser, Thr, Tro, Tyr, Val (2.5 mM). (B) Fluorescence intensity at 665 nm of DCM-S-CPT (10 μM) as a function of pH value in the absence and presence of GSH (2.5 mM) in DMSO/PBS solution (50/50, v/v, pH = 7.4, 10 mM). Each point was recorded after exposure to GSH for 1 h at 37 °C, λ_{ex} = 465 nm.

Response Rate and Photostability. Time-course experiments of DCM-S-CPT and DCM-C-CPT with GSH were conducted. As illustrated in Figure 3A, the fluorescence intensity of DCM-S-CPT at 665 nm gradually increases to a plateau within 1200 s (20 min) in the presence of GSH. The released amount of CPT was found to correlate well with the observed increase in fluorescence intensity at 665 nm by HPLC (Figure 3B and Figure S6 in SI), while in the absence of GSH, neither CPT release nor the fluorescence enhancement at 665 nm was observed. As a control, the constant fluorescence intensity of DCM-C-CPT in the presence of GSH proves the crucial role of the disulfide bond. Here the fluorescence of DCM-S-CPT at 665 nm with its fast response to GSH can act as a direct off−on signal reporter for CPT release.

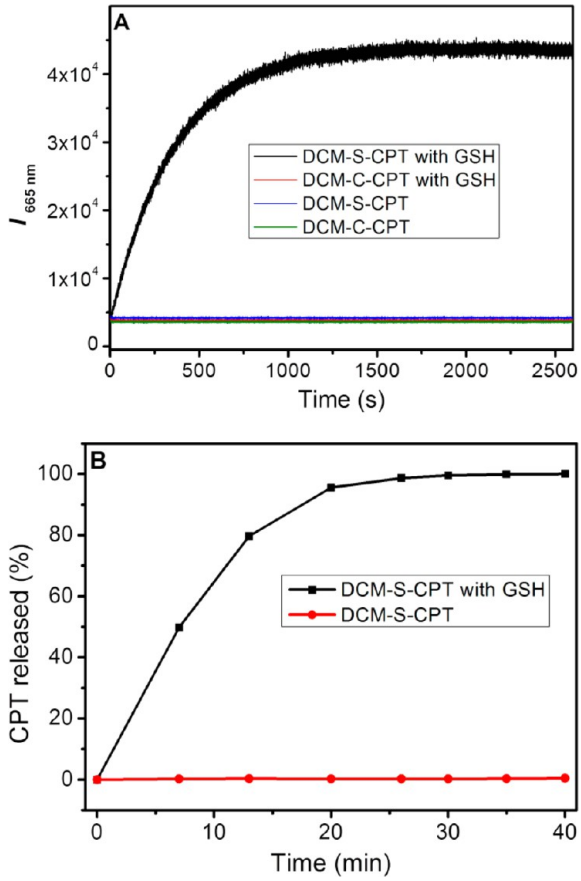

Figure 3. (A) Time dependence of fluorescence intensity at 665 nm for DCM-S-CPT and DCM-C-CPT (10 μM) in DMSO/PBS solution (1:1, v/v, pH = 7.4, 10 mM) in the presence (black and red) and absence (blue and green) of GSH (2.5 mM). λ_{ex} = 465 nm. Data was recorded every 0.5 s. (B) CPT released from DCM-S-CPT as a function of time in the presence and absence of GSH (2.5 mM). CPT in RP (reverse phase)-HPLC chromatograms was detected by UV absorption using 365 nm as the monitored wavelength.

As mentioned above, the photostability of NIR fluorophores in DDS is a crucial element for practical application in bioimaging *in vivo*.[36] The time-dependent fluorescence

dx.doi.org/10.1021/ja412380j | J. Am. Chem. Soc. 2014, 136, 3579−3588

measurements were conducted for the photostability of GSH-treated DCM-S-CPT upon continuous illumination (Hamamatsu, LC8 Lightningcure, 300 W) in DMSO/PBS (50:50, v/v), and compared with cyanine dye ICG (the FDA-approved NIR contrast agent). After exposure for about 100 s, the fluorescence of ICG decreased sharply to approximate 5% of the initial value (monitored at 812 nm, Figure 4), indicative of

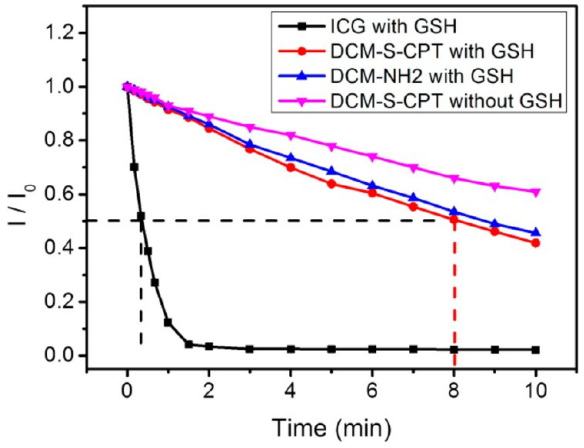

Figure 4. Time-dependent fluorescence intensity of ICG (10 μM in DMSO/PBS = 1:1, treated with 2.5 mM GSH, monitored at 812 nm, and excited at 780 nm), DCM-S-CPT (10 μM in DMSO/PBS = 1:1, treated with 2.5 mM GSH for 1 h at 37 °C, monitored at 665 nm and excited at 465 nm), DCM-NH_2 (10 μM in DMSO/PBS = 1:1, treated with 2.5 mM GSH, monitored at 665 nm and excited at 465 nm), and DCM-S-CPT (10 μM in DMSO/PBS = 1:1, monitored at 665 nm and excited at 465 nm) under illumination.

the almost complete decomposition of the scaffold of ICG, while for DCM-S-CPT in the presence of GSH, more than 80% of the original fluorescence at 665 nm survived (Figure 4). Obviously, DCM-S-CPT on treatment with GSH as well as production of DCM-NH_2 exhibited much better photostability than ICG. As calculated from the time-course fluorescence measurements, the fluorescence half-life of DCM-S-CPT (~470 s) is 19-fold longer than that of ICG (~25 s). The high photostability of DCM-S-CPT indicates that it can be used as an excellent contrast agent for *in vivo* bioimaging.

Cytotoxicity Evaluation and Living Cell Imaging. Given that DCM-S-CPT can be activated to release CPT, we investigated its performance in cell lines *in vitro*. The cytotoxicity of free CPT, DCM-C-CPT, and DCM-S-CPT including their PEG-PLA nanoparticles against a large panel of human tumor cell lines was evaluated using typical MTT assays (Figure 5 and Figure S7 in SI). Compared with the parent drug CPT, DCM-S-CPT showed similar cytotoxicity with significant *in vitro* antitumor activity against cell lines including BCap-37, $HepG_2$, MCF-7, HeLa, KB, and KB_{200}. The IC_{50} (concentration inhibiting cell growth to 50% of control) values of DCM-S-CPT in the above cell lines were 11.1, 14.4, 21.4, 22.5, 4.5, and 2.1 μM, respectively, being slightly higher than that of CPT and around 2-fold lower than that of DCM-C-CPT. Obviously, DCM-S-CPT could release CPT sufficiently by the cleavage of the disulfide linkage upon the uptake by cancer cells, whereas DCM-C-CPT was totally unable to release CPT in cancer cells, resulting in lower cytotoxicity. This perfectly coincides with the spectroscopic results. Furthermore, the parent drug CPT showed obvious cytotoxicity toward noncancerous cells MDCK, whereas DCM-S-CPT, DCM-C-CPT, and their

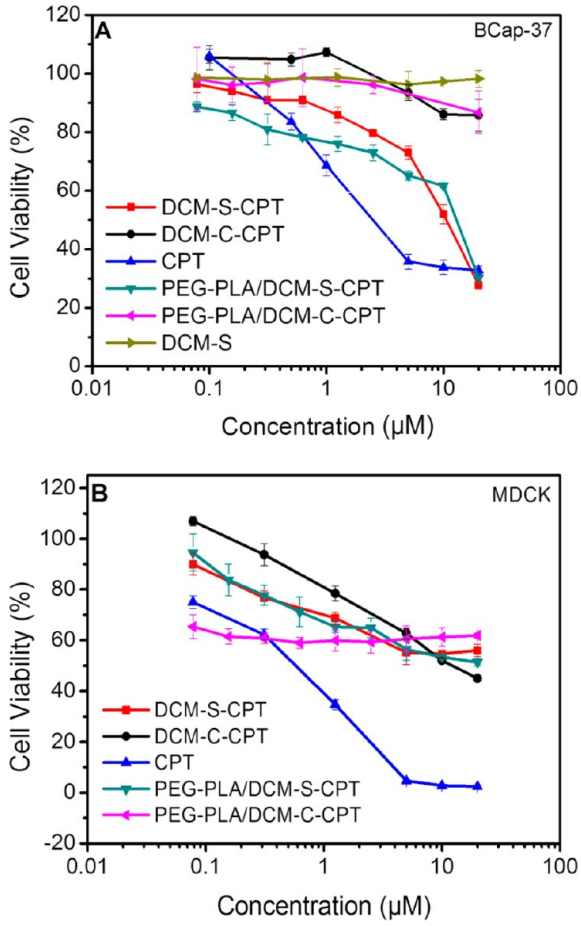

Figure 5. Cytotoxicity of DCM-S-CPT, DCM-C-CPT, CPT, PEG-PLA/DCM-S-CPT, PEG-PLA/DCM-C-CPT, and DCM-S on BCap-37 cancer cells (A) and MDCK cells (B).

PEG-PLA nanoparticles showed much lower cytotoxicity at the same drug concentration. Undoubtedly, DCM-S-CPT released active CPT in cancer cells rather than normal cells because of the much higher concentration of intracellular GSH in cancer cells (Figure 5B).[26,95] Moreover, the PEG-PLA nanoparticles of DCM-S-CPT and DCM-C-CPT showed the same cytotoxicity against cancer cells as the relevant prodrugs, indicative of the ignorable influence of the nanoparticle matrix on the cytotoxicity of the DCM-S-CPT (Figure 5).

The cellular uptake and intracellular localization of DCM-S-CPT and DCM-C-CPT were observed by confocal laser scanning microscopy. The fluorescence from DCM-NH_2 (red) was observed in the cytoplasm after 3 h of incubation at 37 °C, indicating that DCM-S-CPT was quickly taken up by cancer cells and decomposed into DCM-NH_2 and CPT by the intracellular GSH (Figure 6A-D). By adding an extra 2.5 mM GSH in order to accelerate the test, a further enhancement of fluorescence (Figure 6E-H) was observed due to further breakage of the disulfide linkage. In contrast, the fluorescence of DCM-NH_2 was hardly observed in the cells cultured with DCM-C-CPT even with an extra 2.5 mM GSH due to the stable alkane linkage between CPT and the DCM moieties (Figure S8 in SI). As demonstrated, the activatable prodrug DCM-S-CPT with fluorescence switch can be used to monitor the drug release process in cancer cells.

Flow cytometry studies were used to further verify the properties of DCM-S-CPT and DCM-C-CPT in the BCap-37

dx.doi.org/10.1021/ja412380j | J. Am. Chem. Soc. 2014, 136, 3579−3588

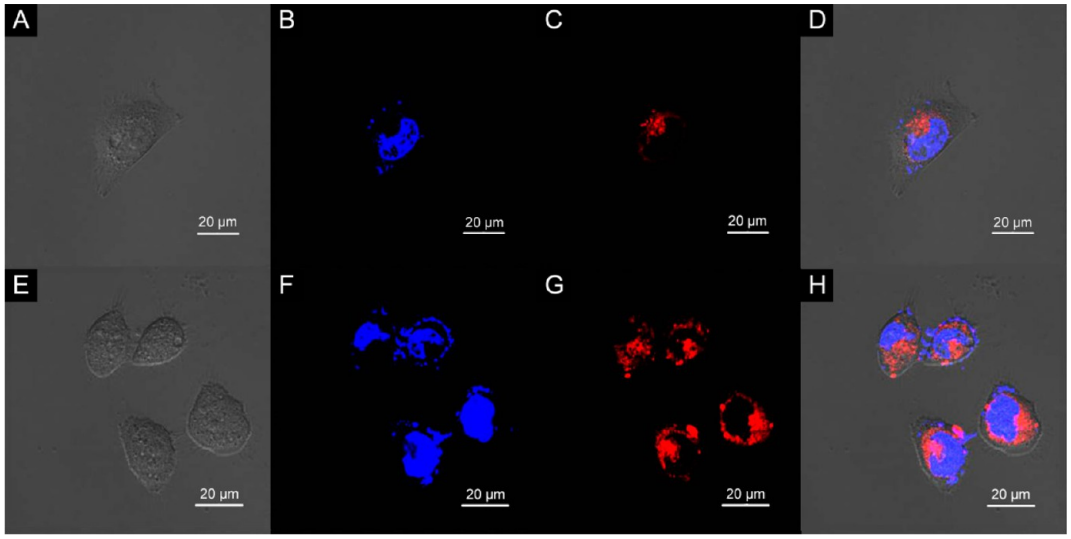

Figure 6. Confocal laser scanning microscopy images of MCF-7 cells cultured with DCM-S-CPT with (E–H) or without (A–D) extra GSH for 3 h. Nucleus was stained with DAPI. Images were taken from the DAPI channel (B and F), DCM-NH_2 channel (C and G), bright field (A and E), and the overlapped image (D and H).

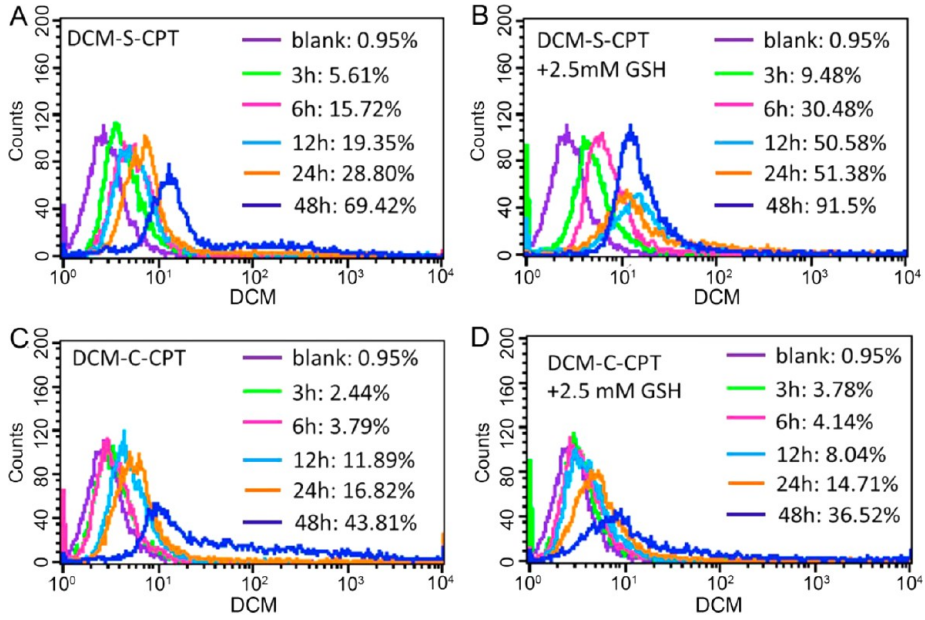

Figure 7. Flow cytometry analysis of cellular uptake of DCM-S-CPT (A and B) and DCM-C–CPT (C and D) at different time intervals from 3 to 48 h in BCap-37 cells with and without extra 2.5 mM GSH.

cell line. The uptake ratios of DCM-S-CPT increased from 5.61% to 69.42% after 3 to 48 h incubation (Figure 7). For the test with an additional 2.5 mM GSH, the uptake ratios dramatically increased to 9.48% and 91.5% after 3 and 48 h incubation. By contrast, the cellular uptake ratio of DCM-C-CPT increased from 2.44% to 43.81% after 3 to 48 h incubation, which is much lower than that of DCM-S-CPT. Unlike DCM-S-CPT, the cellular uptake ratios were 3.78% to 36.52% even upon the addition of an extra 2.5 mM GSH (Figure 7). The enhancement in uptake ratio indicates that, for the activatable prodrug DCM-S-CPT, the incorporated disulfide bond plays a critical role in the intracellular cleavage by the interaction with GSH.

The promising results in living cell imaging inspired us to further explore the feasibility of DCM-S-CPT as an *in vivo* NIR fluorescence-tracked drug delivery system. The *in vivo* drug delivery performance and biodistribution of DCM-S-CPT and DCM-C-CPT were investigated with tumor-bearing mice, intravenously injected with DCM-S-CPT and reference objects using an *in vivo* imaging system. Merely 9 min after the intravenous injection of DCM-S-CPT (0.08 mg/kg), the NIR fluorescence was already clearly observable whereas with DCM-C-CPT the fluorescence was much lower (Figure 8), indicative of the rapid distribution of DCM-S-CPT *via* the blood circulation and the rapid cleavage of the disulfide bond *in vivo*. Intriguingly, after the distribution process, DCM-S-CPT had the strongest fluorescence, as well as the largest amount of released CPT, in the tumor, with much weaker fluorescence in liver, stomach, kidney, and lung, indicating prominent tumor-targeting ability. Probably, the unanticipated targeted drug

dx.doi.org/10.1021/ja412380j | J. Am. Chem. Soc. 2014, 136, 3579–3588

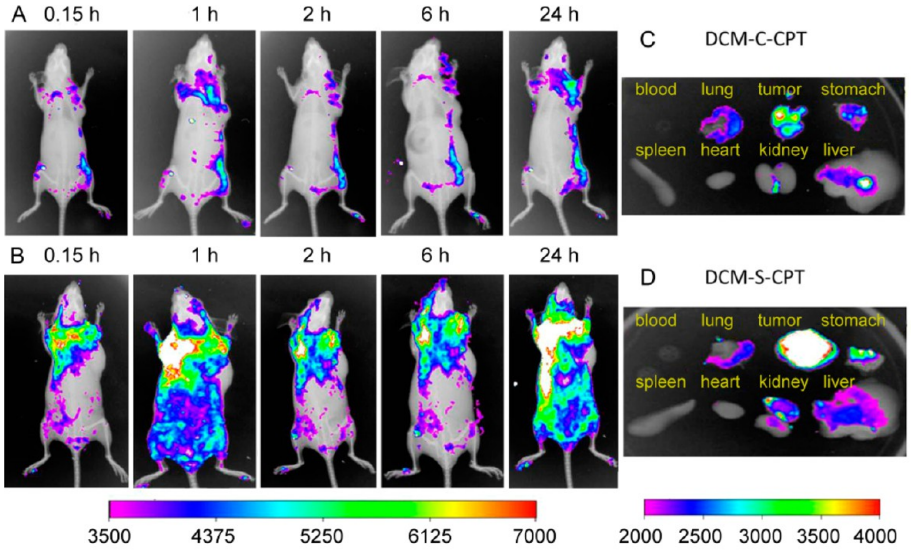

Figure 8. *In vivo* imaging of tumor-bearing mice at various time (0.15, 1, 2, 6, and 24 h) after intravenous injection of (A) DCM-C-CPT (0.08 mg/kg), (B) DCM-S-CPT (0.08 mg/kg), and the fluorescence images of the internal organs after anatomy for (C) DCM-C-CPT and (D) DCM-S-CPT. The color bars correspond to the detected fluorescence intensity.

release along with fluorescence enhancement could be ascribed to the particularly high GSH concentration in cancer cells (Figure 8). The tumor-specificity ability and the specific drug release in tumor make DCM-S-CPT a promising prodrug to achieve high efficacy and reduced side-effects.

Pharmacokinetic Study with PEG-PLA Loaded Prodrug (PEG-PLA/DCM-S-CPT). To get a deeper insight into the anticancer activity and improve the water solubility, the prodrugs were loaded into biodegradable PEG-PLA micelle. The blood clearance kinetics of the resultant PEG-PLA/DCM-S-CPT in comparison with CPT was determined by measuring the blood drug concentration after single intravenous administration of them at a dose equivalent to 5 mg/kg CPT (Figure S9 in SI). While CPT was cleared very quickly, the clearance of the prodrug loaded in PEG-PLA micelle was much slower. There was still 10.7% of the injected dose in blood with the PEG-PLA/DCM-S-CPT 24 h after treatment, whereas CPT was barely detected in the blood at the same time point. Notably, during the entire blood clearance process of 24 h, the blood drug concentration in the case of PEG-PLA/DCM-S-CPT was always larger than free CPT. These data clearly demonstrate that the encapsulation of DCM-S-CPT using PEG-PLA micelle results in a slower blood clearance, which favors passive accumulation in the tumor *via* EPR effect.[84]

Subsequently, to investigate the *in vivo* biodistribution and drug release of the encapsulated prodrugs, nude mice were intravenously injected with PEG-PLA/DCM-S-CPT and PEG-PLA/DCM-C-CPT at a dose of 5 mg/kg. Not surprisingly, NIR fluorescence representing the release of active CPT was retained in the tumor even 24 h after the injection (Figure S10 in SI). The long retention of PEG-PLA/DCM-S-CPT in the tumor, which is probably attributed to the EPR effect, makes this system very promising for tumor labeling and tumor chemotherapy. Furthermore, the confocal image of a tumor slice (10 μm thick) sectioned from the mouse treated with PEG-PLA/DCM-S-CPT clearly exhibited strong and homogeneously distributed NIR fluorescence, whereas that from the mouse treated with PEG-PLA/DCM-C-CPT showed weak and uneven fluorescence (Figure S11 in SI), which is consistent with the findings from the *in vivo* imaging studies. This further proves that PEG-PLA/DCM-S-CPT could penetrate deeply into the tumor and release DCM-S-CPT after the endocytosis of nanoparticles into cancer cells followed by cleavage of the disulfide bond to release DCM-NH_2 and CPT.

Antitumor Activity. The *in vivo* antitumor activities were compared using BCap-37 tumor xenograft model. Mice bearing the tumors were intravenously treated with PBS, CPT, PEG-PLA/DCM-S-CPT, and PEG-PLA/DCM-C-CPT at a CPT-equivalent dose of 5 mg/kg (Figure 9). Obviously, the treatments of CPT or PEG-PLA/DCM-S-CPT led to significant inhibition of BCap-37 tumor growth compared to the control group (PBS, Figure 9A). The inhibition rates of tumor growth (IRT) of CPT, PEG-PLA/DCM-S-CPT, and PEG-PLA/DCM-C-CPT on BCap-37 tumors were 88.9%, 96.4%, and 16.3%, respectively (Figure 9C). Remarkably, PEG-PLA/DCM-S-CPT induced even higher IRTs than free CPT, and certainly than PEG-PLA/DCM-C-CPT ($p < 0.01$). Meanwhile, the tumor images were consistent with the IRT data (Figure 9D). Otherwise, the body weights of all the mice gradually increased except the CPT-treated group throughout the experiments (Figure 9B), indicating that the PEG-PLA loaded nanoparticles-treated groups did not cause severe systematic side effects, whereas CPT could lead to toxicity in mice.

Finally, the removed BCap-37 xenograft tumors were fixed and prepared for histological analysis. In the control group (PBS treated), the tumor tissue sections were composed of tightly packed tumor cells interspersed with various amounts of stroma, while apoptotic tumor cells were rarely observed (Figure 9E). After the treatment with PEG-PLA/DCM-S-CPT and CPT, the histological features of tumors exhibited significant differences from the control group. For example, a large amount of tumor cells became much larger after treatment with PEG-PLA/DCM-S-CPT, and the tumor cellularity, as evaluated by average tumor cell numbers of each microscopic field, reduced significantly when compared with the control group. In addition, many tumor cells exhibited vacuolization and typical apoptotic characteristics; that is, they were composed of membrane-bound and small nuclear fragments surrounded by a rim of cytoplasm. The tumors treated with

dx.doi.org/10.1021/ja412380j | J. Am. Chem. Soc. 2014, 136, 3579−3588

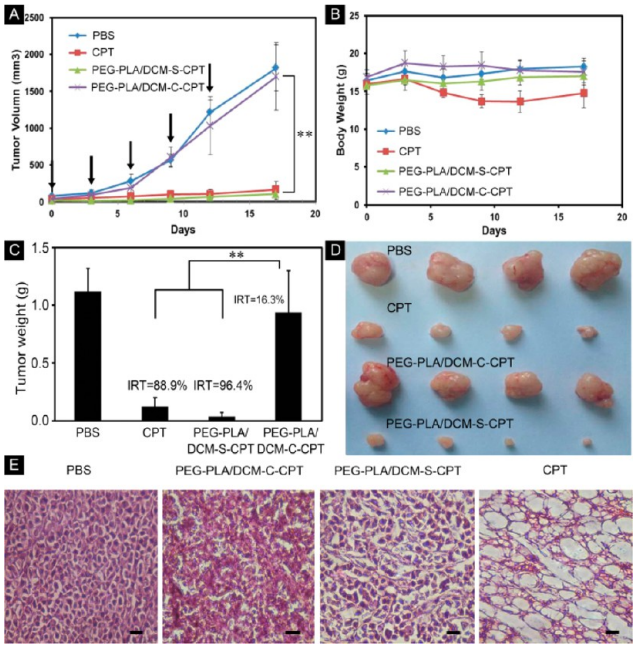

Figure 9. Antitumor activities of PBS, CPT, PEG-PLA/DCM-S-CPT, and PEG-PLA/DCM-C-CPT i.v. administered at a CPT-equivalent dose of 5 mg/kg every 3 days, as indicated by the arrows, against BCap-37 xenograft tumors ($n = 4$, data expressed as average ± SE, * or ** means $P < 0.05$ or 0.01, respectively). The results are summarized as tumor volumes of mice bearing BCap-37 tumors exposed to various treatments (A), the body weight changes (B), the tumor weights of each group of the mice at the end of the experiment and inhibition rates of tumor growth (IRT) (*, $p < 0.05$; and **, $p < 0.01$) (C), the image of tumors (D), and representative histological features of BCap-37 tumors from the treated mice (scale bar = 50 μm) (E).

PEG-PLA/DCM-S-CPT and CPT also had significantly lower tumor cellularity and more apoptotic cells than that treated with PEG-PLA/DCM-C-CPT (Figure 9D), which was consistent with the higher IRT induced by PEG-PLA/DCM-S-CPT and CPT than PEG-PLA/DCM-C-CPT.

CONCLUSIONS

In summary, we have developed a novel activatable NIR theranostic prodrug platform based on the DCM chromophore for *in vivo* and *in situ* monitoring of cancer chemotherapy in living animals, wherein both the fluorescence and cytotoxicity of the drug (CPT) are quenched by the covalent disulfide linker. The prodrug DCM-S-CPT and its PEG-PLA loaded nanoparticles become NIR turn-on fluorescent and cytotoxic upon the specific GSH-induced cleavage of the disulfide bond. Flow cytometric analysis confirms that DCM-S-CPT is endocytosed into the cells to release the active CPT as well as the NIR fluorescence. The most striking feature of NIR prodrug DCM-S-CPT is its excellent specific tumor-activatable performance in tumor-bearing nude mice. The prodrug-encapsulated nanoparticles of PEG-PLA/DCM-S-CPT also display significantly enhanced *in vivo* antitumor activity with lower side effects in comparison with free CPT. Impressively, the excellent NIR fluorescence and photostability of the DCM chromophore with large Stokes shift make it possible to implement *in vivo* and *in situ* tracking drug release and cancer therapeutic efficacy in living animals, being capable of deeply penetrating skin and overlaying tissue with low background interference. Thus, our work illustrates a promising NIR DCM-based prodrug platform for specific tumor-activatable drug delivery systems. The feature of DCM-S-CPT for *in situ* and *in vivo* tracking of drug release and cancer therapeutic efficacy in living cells and animals provides a significant advance toward deeper understanding and exploration of theranostic drug-delivery systems.

ASSOCIATED CONTENT

Supporting Information

More detailed experimental procedures, characterizations, supplementary optical spectra and figures. This material is available free of charge via the Internet at http://pubs.acs.org.

AUTHOR INFORMATION

Corresponding Authors

*E-mail: whzhu@ecust.edu.cn.
*E-mail: guozq@ecust.edu.cn.
*E-mail: jianbin@zju.edu.cn.

Author Contributions

X.M.W. and X.R.S. contributed equally.

Notes

The authors declare no competing financial interest.

ACKNOWLEDGMENTS

This work was supported by National 973 Program (2013CB733700), NSFC/China, NSFC for Distinguished Young Scholars (Grant No. 21325625), the Oriental Scholarship, National Major Scientific Technological Special Project (2012YQ15008709), SRFDP 20120074110002, Shanghai Pujiang Program (13PJD010), the Fundamental Research Funds for the Central Universities (WK1013002, WJ1114013, 222201313010), and Open Funding Project of the State Key Laboratory of Bioreactor Engineering. The Catalysis And Sensing for our Environment (CASE) network is thanked for research exchange opportunities. T.D.J. thanks ECUST for a guest professorship.

REFERENCES

(1) Atkins, J. H.; Gershell, L. J. *Nat. Rev. Cancer* **2002**, *2*, 645−646.
(2) Irvine, D. J. *Nat. Mater.* **2011**, *10*, 342−343.
(3) Hubbell, J. A.; Langer, R. *Nat. Mater.* **2013**, *12*, 963−966.
(4) Mura, S.; Nicolas, J.; Couvreur, P. *Nat. Mater.* **2013**, *12*, 991−1003.
(5) Mahato, R.; Tai, W.; Cheng, K. *Adv. Drug Delivery Rev.* **2011**, *63*, 659−670.
(6) Zhang, S.; Chan, K. H.; Prud'Homme, R. K.; Link, A. J. *Mol. Pharm.* **2012**, *9*, 2228−2236.
(7) Kim, E.; Kim, D.; Jung, H.; Lee, J.; Paul, S.; Selvapalam, N.; Yang, Y.; Lim, N.; Park, C. G.; Kim, K. *Angew. Chem., Int. Ed.* **2010**, *49*, 4405−4408.
(8) Cafeo, G.; Carbotti, G.; Cuzzola, A.; Fabbi, M.; Ferrini, S.; Kohnke, F. H.; Papanikolaou, G.; Plutino, M. R.; Rosano, C.; White, A. J. P. *J. Am. Chem. Soc.* **2013**, *135*, 2544−2551.
(9) Danhier, F.; Feron, O.; Préat, V. *J. Controlled Release* **2010**, *148*, 135−146.
(10) Kwon, I. K.; Lee, S. C.; Han, B.; Park, K. *J. Controlled Release* **2012**, *164*, 108−114.
(11) Meng, H.; Xue, M.; Xia, T.; Zhao, Y.; Tamanoi, F.; Stoddart, J. F.; Zink, J. I.; Nel, A. E. *J. Am. Chem. Soc.* **2010**, *132*, 12690−12697.
(12) Frasconi, M.; Liu, Z.; Lei, J.; Wu, Y.; Strekalova, E.; Malin, D.; Ambrogio, M. W.; Chen, X.; Botros, Y. Y.; Cryns, V. L.; Sauvage, J.; Stoddart, J. F. *J. Am. Chem. Soc.* **2013**, *135*, 11603−11613.
(13) Meng, F.; Zhong, Z.; Jan, F. J. *Biomacromolecules* **2009**, *10*, 197−209.

(14) Jin, E. L.; Zhang, B.; Sun, X. R.; Zhou, Z. X.; Ma, X. P.; Sun, Q. H.; Tang, J. B.; Shen, Y. Q.; Van Kirk, E.; Murdoch, W. J.; Radosz, M. *J. Am. Chem. Soc.* **2013**, *135*, 933−940.
(15) Duan, Q. P.; Cao, Y.; Li, Y.; Hu, X. Y.; Xiao, T. X.; Lin, C.; Pan, Y.; Wang, L. Y. *J. Am. Chem. Soc.* **2013**, *135*, 10542−10549.
(16) Liu, J.; Pang, Y.; Huang, W.; Huang, X.; Meng, L.; Zhu, X.; Zhou, Y.; Yan, D. *Biomacromolecules* **2011**, *12*, 1567−1577.
(17) Santra, S.; Kaittanis, C.; Santiesteban, O. J.; Perez, J. M. *J. Am. Chem. Soc.* **2011**, *133*, 16680−16688.
(18) Shen, Y. Q.; Jin, E. L.; Zhang, B.; Murphy, C. J.; Sui, M. H.; Zhao, J.; Wang, J. Q.; Tang, J. B.; Fan, M. H.; Van Kirk, E.; Murdoch, W. J. *J. Am. Chem. Soc.* **2010**, *132*, 4259−4265.
(19) Ge, Z. S.; Liu, S. Y. *Chem. Soc. Rev.* **2013**, *42*, 7289−7325.
(20) Banerjee, S.; Kar, S.; Perez, J. M.; Santra, S. *J. Phys. Chem. C* **2009**, *113*, 9659−9663.
(21) Ducry, L.; Stump, B. *Bioconjugate Chem.* **2009**, *21*, 5−13.
(22) McMahon, B. K.; Gunnlaugsson, T. *J. Am. Chem. Soc.* **2012**, *134*, 10725−10728.
(23) Niu, L. Y.; Guan, Y. S.; Chen, Y. Z.; Wu, L. Z.; Tung, C. H.; Yang, Q. Z. *J. Am. Chem. Soc.* **2012**, *134*, 18928−18931.
(24) El Alaoui, A.; Schmidt, F.; Amessou, M.; Sarr, M.; Decaudin, D.; Florent, J.; Johannes, L. *Angew. Chem., Int. Ed.* **2007**, *46*, 6469−6472.
(25) Zhou, Z. X.; Shen, Y. Q.; Tang, J. B.; Fan, M.; Van Kirk, E. A.; Murdoch, W. J.; Radosz, M. *Adv. Funct. Mater.* **2009**, *19*, 3580−3589.
(26) Lee, M. H.; Yang, Z.; Lim, C. W.; Lee, Y. H.; Dongbang, S.; Kang, C.; Kim, J. S. *Chem. Rev.* **2013**, *113*, 5071−5109.
(27) Zhao, Z.; Meng, H.; Wang, N.; Donovan, M. J.; Fu, T.; You, M.; Chen, Z.; Zhang, X.; Tan, W. *Angew. Chem., Int. Ed.* **2013**, *52*, 7487−7491.
(28) Andersen, E. S.; Dong, M.; Nielsen, M. M.; Jahn, K.; Subramani, R.; Mamdouh, W.; Golas, M. M.; Sander, B.; Stark, H.; Oliveira, C. L. P.; Pedersen, J. S.; Birkedal, V.; Besenbacher, F.; Gothelf, K. V.; Kjems, J. *Nature* **2009**, *459*, 73−76.
(29) Zhang, J.; Yuan, Z. F.; Wang, Y.; Chen, W. H.; Luo, G. F.; Cheng, S. X.; Zhuo, R. X.; Zhang, X. Z. *J. Am. Chem. Soc.* **2013**, *135*, 5068−5073.
(30) Gorityala, B. K.; Lu, Z.; Leow, M. L.; Ma, J.; Liu, X. *J. Am. Chem. Soc.* **2012**, *134*, 15229−15232.
(31) Lee, S.; Chen, H.; O Halloran, T. V.; Nguyen, S. T. *J. Am. Chem. Soc.* **2009**, *131*, 9311−9320.
(32) Chevalier, A.; Dubois, M.; Le Joncour, V.; Dautrey, S.; Lecointre, C.; Romieu, A.; Renard, P.; Castel, H.; Sabot, C. *Bioconjugate Chem.* **2013**, *24*, 1119−1133.
(33) Geng, Q.; Sun, X.; Gong, T.; Zhang, Z. *Bioconjugate Chem.* **2012**, *23*, 1200−1210.
(34) Shi, H.; Kwok, R. T. K.; Liu, J.; Xing, B.; Tang, B. Z.; Liu, B. *J. Am. Chem. Soc.* **2012**, *134*, 17972−17981.
(35) Frangioni, J. V. *Curr. Opin. Chem. Biol.* **2003**, *7*, 626−634.
(36) Wu, X. M.; Chang, S.; Sun, X. R.; Guo, Z. Q.; Li, Y. S.; Tang, J. B.; Shen, Y. Q.; Shi, J. L.; Tian, H.; Zhu, W. H. *Chem. Sci.* **2013**, *4*, 1221−1228.
(37) Yang, Y. M.; Zhao, Q.; Feng, W.; Li, F. Y. *Chem. Rev.* **2012**, *113*, 192−270.
(38) Jin, P. W.; Chu, J.; Miao, Y.; Tan, J.; Zhang, S. L.; Zhu, W. H. *AIChE J.* **2013**, *59*, 2743−2752.
(39) Jin, P.; Guo, Z. Q.; Chu, J.; Tan, J.; Zhang, S. L.; Zhu, W. H. *Ind. Eng. Chem. Res.* **2013**, *52*, 3980−3987.
(40) Wang, X.; Cui, L.; Zhou, N.; Zhu, W.; Wang, R.; Qian, X. H.; Xu, Y. F. *Chem. Sci.* **2013**, *4*, 2936−2940.
(41) Geng, J.; Li, K.; Ding, D.; Zhang, X.; Qin, W.; Liu, J.; Tang, B. Z.; Liu, B. *Small* **2012**, *8*, 3655−3663.
(42) Myochin, T.; Kiyose, K.; Hanaoka, K.; Kojima, H.; Terai, T.; Nagano, T. *J. Am. Chem. Soc.* **2011**, *133*, 3401−3409.
(43) Guo, Z. Q.; Park, S.; Yoon, J.; Shin, I. *Chem. Soc. Rev.* **2014**, *43*, 16−29.
(44) Liu, Y.; Chen, M.; Cao, T. Y.; Sun, Y.; Li, C. Y.; Liu, Q.; Yang, T. S.; Yao, L. M.; Feng, W.; Li, F. Y. *J. Am. Chem. Soc.* **2013**, *135*, 9869−9876.
(45) Xin, J.; Zhang, X.; Liang, J.; Xia, L.; Yin, J.; Nie, Y.; Wu, K.; Tian, J. *Bioconjugate Chem.* **2013**, *24*, 1134−1143.
(46) Yuan, L.; Lin, W. Y.; Zhao, S.; Gao, W. S.; Chen, B.; He, L. W.; Zhu, S. S. *J. Am. Chem. Soc.* **2012**, *134*, 13510−13523.
(47) Truman, L. K.; Comby, S.; Gunnlaugsson, T. *Angew. Chem., Int. Ed.* **2012**, *51*, 9624−9627.
(48) Palma, A.; Alvarez, L. A.; Scholz, D.; Frimannsson, D. O.; Grossi, M.; Quinn, S. J.; O Shea, D. F. *J. Am. Chem. Soc.* **2011**, *133*, 19618−19621.
(49) Batat, P.; Cantuel, M.; Jonusauskas, G.; Scarpantonio, L.; Palma, A.; O Shea, D. F.; McClenaghan, N. D. *J. Phys. Chem. A* **2011**, *115*, 14034−14039.
(50) Maiti, S.; Park, N.; Han, J. H.; Jeon, H. M.; Lee, J. H.; Bhuniya, S.; Kang, C.; Kim, J. S. *J. Am. Chem. Soc.* **2013**, *135*, 4567−4572.
(51) Lee, M. H.; Kim, J. Y.; Han, J. H.; Bhuniya, S.; Sessler, J. L.; Kang, C.; Kim, J. S. *J. Am. Chem. Soc.* **2012**, *134*, 12668−12674.
(52) Banerjee, S.; Veale, E. B.; Phelan, C. M.; Murphy, S. A.; Tocci, G. M.; Gillespie, L. J.; Frimannsson, D. O.; Kelly, J. M.; Gunnlaugsson, T. *Chem. Soc. Rev.* **2013**, *42*, 1601−1618.
(53) Yang, Z.; Lee, J. H.; Jeon, H. M.; Han, J. H.; Park, N.; He, Y.; Lee, H.; Hong, K. S.; Kang, C.; Kim, J. S. *J. Am. Chem. Soc.* **2013**, *135*, 11657−11662.
(54) Shank, N. I.; Pham, H. H.; Waggoner, A. S.; Armitage, B. A. *J. Am. Chem. Soc.* **2012**, *135*, 242−251.
(55) Altman, R. B.; Terry, D. S.; Zhou, Z.; Zheng, Q.; Geggier, P.; Kolster, R. A.; Zhao, Y.; Javitch, J. A.; Warren, J. D.; Blanchard, S. C. *Nat. Methods* **2012**, *9*, 68−71.
(56) Samanta, A.; Vendrell, M.; Das, R.; Chang, Y. *Chem. Commun.* **2010**, *46*, 7406−7408.
(57) Guo, Z. Q.; Zhu, W. H.; Tian, H. *Chem. Commun.* **2012**, *48*, 6073−6084.
(58) Zhu, W. H.; Huang, X. M.; Guo, Z. Q.; Wu, X. M.; Yu, H. H.; Tian, H. *Chem. Commun.* **2012**, *48*, 1784−1786.
(59) Tong, H.; Hong, Y.; Dong, Y.; Ren, Y.; Häussler, M.; Lam, J. W. Y.; Wong, K. S.; Tang, B. Z. *J. Phys. Chem. B* **2007**, *111*, 2000−2007.
(60) Barbon, A.; Bott, E. D.; Brustolon, M.; Fabris, M.; Kahr, B.; Kaminsky, W.; Reid, P. J.; Wong, S. M.; Wustholz, K. L.; Zanré, R. *J. Am. Chem. Soc.* **2009**, *131*, 11548−11557.
(61) Sun, W.; Fan, J.; Hu, C.; Cao, J.; Zhang, H.; Xiong, X.; Wang, J.; Cui, S.; Sun, S.; Peng, X. J. *Chem. Commun.* **2013**, *49*, 3890−3892.
(62) Huang, X. M.; Guo, Z. Q.; Zhu, W. H.; Xie, Y. S.; Tian, H. *Chem. Commun.* **2008**, 5143−5145.
(63) Guo, Z. Q.; Zhu, W. H.; Tian, H. *Macromolecules* **2010**, *43*, 739−744.
(64) Guo, Z. Q.; Zhao, P.; Zhu, W. H.; Huang, X. M.; Xie, Y. S.; Tian, H. *J. Phys. Chem. C* **2008**, *112*, 7047−7053.
(65) Guo, Z. Q.; Zhu, W. H.; Shen, L. J.; Tian, H. *Angew. Chem., Int. Ed.* **2007**, *46*, 5549−5553.
(66) Liu, B.; Zhu, W. H.; Zhang, Q.; Wu, W. J.; Xu, M.; Ning, Z. J.; Xie, Y. S.; Tian, H. *Chem. Commun.* **2009**, 1766−1768.
(67) Liu, B.; Li, X. Y.; Liu, M. Y.; Ning, Z. J.; Zhang, Q.; Li, C.; Müllen, K.; Zhu, W. H. *Dyes Pigm.* **2012**, *94*, 23−27.
(68) Hsiang, Y.; Liu, L. F.; Wall, M. E.; Wani, M. C.; Nicholas, A. W.; Manikumar, G.; Kirschenbaum, S.; Silber, R.; Potmesil, M. *Cancer Res.* **1989**, *49*, 4385−4389.
(69) Moon, S.; Govindan, S. V.; Cardillo, T. M.; D Souza, C. A.; Hansen, H. J.; Goldenberg, D. M. *J. Med. Chem.* **2008**, *51*, 6916−6926.
(70) Lee, M. H.; Han, J. H.; Kwon, P.; Bhuniya, S.; Kim, J. Y.; Sessler, J. L.; Kang, C.; Kim, J. S. *J. Am. Chem. Soc.* **2011**, *134*, 1316−1322.
(71) Reddie, K. G.; Humphries, W. H.; Bain, C. P.; Payne, C. K.; Kemp, M. L.; Murthy, N. *Org. Lett.* **2012**, *14*, 680−683.
(72) Lee, M. H.; Han, J. H.; Lee, J.; Choi, H. G.; Kang, C.; Kim, J. S. *J. Am. Chem. Soc.* **2012**, *134*, 17314−17319.
(73) Kumar, V.; Anslyn, E. V. *J. Am. Chem. Soc.* **2013**, *135*, 6338−6344.
(74) Jiang, W.; Fu, Q.; Fan, H.; Ho, J.; Wang, W. *Angew. Chem., Int. Ed.* **2007**, *46*, 8445−8448.
(75) Xuan, W.; Sheng, C.; Cao, Y.; He, W.; Wang, W. *Angew. Chem., Int. Ed.* **2012**, *51*, 2282−2284.

(76) Chen, X. Q.; Zhou, Y.; Peng, X. J.; Yoon, J. *Chem. Soc. Rev.* **2010**, *39*, 2120−2135.
(77) Kang, B.; Afifi, M. M.; Austin, L. A.; El-Sayed, M. A. *ACS Nano* **2013**, *7*, 7420−7427.
(78) Kreuz, C.; Chang, J.; Hwang, Y. K.; Marsaud, V.; Bories, P.; Cynober, L.; Gil, S.; Ferey, G.; Couvreur, P.; Gref, R. *Nat. Mater.* **2010**, *9*, 172−178.
(79) Horcajada, P.; Chalati, T.; Serre, C.; Gillet, B.; Sebrie, C.; Baati, T.; Eubank, J. F.; Heurtaux, D.; Clayette, P.; Ma, X. P.; Zhou, Z. X.; Jin, E. L.; Sun, Q. H.; Zhang, B.; Tang, J. B.; Shen, Y. Q. *Macromolecules* **2012**, *46*, 37−42.
(80) Hammond, P. R. *Opt. Commun.* **1979**, *29*, 331−333.
(81) Bourson, J.; Valeur, B. *J. Phys. Chem.* **1989**, *93*, 3871−3876.
(82) Grimes, K. D.; Gupte, A.; Aldrich, C. C. *Synthesis* **2010**, 1441−1448.
(83) Chung, C.; Srikun, D.; Lim, C. S.; Chang, C. J.; Cho, B. R. *Chem. Commun.* **2011**, *47*, 9618−9620.
(84) Fang, J.; Nakamura, H.; Maeda, H. *Adv. Drug Delivery Rev.* **2011**, *63*, 136−151.
(85) Yang, J.; Sun, X. R.; Mao, W. W.; Sui, M. H.; Tang, J. B.; Shen, Y. Q. *Mol. Pharm.* **2012**, *9*, 2793−2800.
(86) Pang, Y.; Liu, J.; Wu, J.; Li, G.; Wang, R.; Su, Y.; He, P.; Zhu, X.; Yan, D.; Zhu, B. *Bioconjugate Chem.* **2010**, *21*, 2093−2102.
(87) Chauhan, V. P.; Jain, R. K. *Nat. Mater.* **2013**, *12*, 958−962.
(88) di Nunzio, M. R.; Cohen, B.; Douhal, A. *J. Phys. Chem. A* **2011**, *115*, 5094−5104.
(89) Fan, J.; Zhan, P.; Hu, M.; Sun, W.; Tang, J.; Wang, J.; Sun, S.; Song, F.; Peng, X. J. *Org. Lett.* **2013**, *15*, 492−495.
(90) Shao, J.; Sun, H.; Guo, H.; Ji, S.; Zhao, J.; Wu, W.; Yuan, X.; Zhang, C.; James, T. D. *Chem. Sci.* **2012**, *3*, 1049−1061.
(91) Hu, X. L.; Hu, J. M.; Tian, J.; Ge, Z. S.; Zhang, G. Y.; Luo, K. F.; Liu, S. Y. *J. Am. Chem. Soc.* **2013**, *135*, 17617−17629.
(92) Ji, S.; Guo, H.; Yuan, X.; Li, X.; Ding, H.; Gao, P.; Zhao, C.; Wu, W.; Wu, W.; Zhao, J. *Org. Lett.* **2010**, *12*, 2876−2879.
(93) Lin, W.; Yuan, L.; Cao, Z.; Feng, Y.; Song, J. *Angew. Chem., Int. Ed.* **2010**, *49*, 375−379.
(94) Li, Y. H.; Zhang, G. X.; Yang, G.; Guo, Y. L; Di, C. A.; Chen, X.; Liu, Z. T.; Liu, H. Y.; Xu, Z. Z.; Xu, W.; Fu, H. B.; Zhang, D. Q. *J. Org. Chem.* **2013**, *78*, 2926−2934.
(95) Hou, Y.; Guo, Z.; Li, J.; Wang, P. G. *Biochem. Biophys. Res. Commun.* **1996**, *228*, 88−93.